

Thermo-Optically Induced Transparency on a photonic chip

Marco Clementi,^{1*} Simone Iadanza,^{2,3} Sebastian Schulz,⁴
Giulia Urbinati,¹ Dario Gerace,¹ Liam O'Faloain,^{2,3} Matteo Galli¹

¹Dipartimento di Fisica, Università di Pavia, Via A. Bassi 6, 27100 Pavia, Italy

²Centre for Advanced Photonics and Process Analysis, Cork Institute of Technology,
Rossa Ave Bishopstown, Cork T12P928, Ireland

³Photonics, Tyndall National Institute, Lee Maltings Complex Dyke Parade,
Cork T12 R5CP, Ireland

⁴SUPA, School of Physics and Astronomy, University of St. Andrews,
Fife KY16 9SS, UK

*e-mail: marco.clementi01@universitadipavia.it

Controlling the optical response of a medium through suitably tuned coherent electromagnetic fields is highly relevant in a number of potential applications, from all-optical modulators to optical storage devices. In particular, electromagnetically induced transparency (EIT) is an established phenomenon in which destructive quantum interference creates a transparency window over a narrow spectral range around an absorption line, which, in turn, allows to slow and ultimately stop light due to the anomalous refractive index dispersion. Here we report on the observation of a

new form of either induced transparency or amplification of a weak probe beam in a strongly driven silicon photonic crystal resonator at room temperature. The effect is based on the oscillating temperature field induced in a nonlinear optical cavity, and it reproduces many of the key features of EIT while being independent of either atomic or mechanical resonances. Such thermo-optically induced transparency (TOIT) will allow a versatile implementation of EIT-analogues in an integrated photonic platform, at almost arbitrary wavelength of interest, room temperature and in a practical, low cost and scalable system.

1 Introduction

Electromagnetically induced transparency (EIT) is a coherent phenomenon in which a control laser induces transparency for a weaker probe laser in an otherwise opaque (or optically thick) medium (1). The effect was first observed in atomic vapours (2), and then exploited to slow the propagation speed of light pulses down to 17 m/s in ultracold atom clouds (3), before achieving stopped light through dynamical control of the pump laser (4). However, EIT experiments typically require complicated set-up configurations and very low operating temperatures. Thus related and analogous effects such as coherent population oscillations (CPO) (5), coupled resonator structures (6), Brillouin-scattering induced transparency (BSIT) (7) and opto-mechanically induced transparency (OMIT) (8, 9, 10) have been investigated. These effects have in common that they rely on the beating or resonant coupling between two optical modes and a set of atomic or mechanical resonances. The very narrow linewidth of the atomic or mechanical resonances leads to a rapidly varying refractive index and hence a potentially large positive or negative group index, given by $n_g = c \frac{\partial k}{\partial \omega}$. This increased group index can be used for applications such

as μ s-scale optical delay (7) or improved performance of deep tissue imaging systems (11). However, both EIT and CPO are resonant phenomena, linked to specific atomic transitions, limiting the wavelength range at which these effects can be realised. Similarly, BSIT and OMIT require structures that support acoustic or mechanical modes. While these approaches can achieve large delays (μ s) this comes at the cost of complex structures and device design.

More recently, a new approach based on photo-thermal effects has been presented (12) in which the heating of a mirror in a table-top two-mirror Fabry-Pérot cavity acts as an effective opto-mechanical coupling by changing the physical length of the cavity, eliminating the need for a mechanical resonance. The use of thermal nonlinearities is an important breakthrough that provides new routes to realisation of induced transparencies. The system relies on a weak photo-thermal effect that is enhanced using a resonance with a quality factor of $Q \approx 5 \times 10^8$ and excitation powers of $10 - 100$ mW.

Here we present a thermo-optically induced transparency (TOIT), based on the temperature-dependent refractive index in an integrated, photonic crystal (PhC) cavity, coherently driven by the beating of a pump-probe beam. Our approach differs from that of Ma *et al* (12), in that the complete microcavity is heated, demonstrating that the use of thermal fields for induced transparency is a general effect, independent of the details of the cavity implementation. The integrated format, working at room temperature, both provides a route to applications and creates more options for engineering the heat dissipation from the cavity and thus manipulating the thermal response times.

In contrast with many EIT analogues, our device is realized in a CMOS-compatible platform with an optical mode volume of $0.27 \mu\text{m}^3$ and operates at room temperature. In addition, the integrated silicon photonic platform is well suited for the realization of induced transparency by thermo-optical nonlinearity, which only requires a singly resonant

cavity, with moderate quality factor ($Q = 38,000$ is used in this work), and microwatt-level coupled power (about 1 million times smaller than previously used), yielding microsecond scale optical delays in conventional microresonators. We present a full theoretical model and a clear experimental demonstration of the TOIT phenomenon. Furthermore, we give an outlook for potential future directions of the field. In particular, we show how the thermal response, and hence the induced transparency linewidth and group delay, of such PhC cavities can be engineered.

2 Theory

Our experiment consists of an optical cavity displaying a self-induced frequency shift due to the thermo-optic effect, as caused by the weak optical absorption from the cavity material (Fig. 1a), which generates free carriers that recombine releasing heat. For such a cavity, the thermo-optically shifted resonance is given by $\bar{\omega}_0 = \omega_0 + \omega_0\alpha\Delta T$, where ω_0 is the “cold” (unperturbed) cavity resonance frequency, $\alpha = \frac{1}{\omega_0} \frac{\partial \omega_0}{\partial T}$ is the refractive index temperature coefficient, and ΔT is the effective temperature offset of the cavity medium due to optical material absorption, with respect to the environment. In analogy to the formalism already introduced to interpret OMIT (9), one can define a thermo-optical coupling parameter $G = \omega_0\alpha$ such that $G\Delta T$ represents the frequency shift due to coupling of the optical mode to the thermal field.

First, we hereby give a physical interpretation of the phenomenon. We are considering the situation in which an intense control beam induces an intracavity field amplitude $\bar{a}e^{i\omega_c t}$ oscillating at frequency $\omega_c = \omega_0 + \Delta$, slightly detuned from the cold cavity resonance. The intracavity energy $|\bar{a}|^2$ gives rise to the steady temperature increase $\overline{\Delta T}$, which in turn leads to a detuning from the “hot” (shifted) cavity resonance $\overline{\Delta} = \omega_c - \bar{\omega}_0$. In this situation, the cavity reaches the thermal equilibrium thanks to heat dissipation to the thermal bath

with a rate γ_{th} ¹.

A second weak laser at a frequency $\omega_p = \omega_c - \Omega$ is used to probe the cavity response, generating a driving field that oscillates at the beating frequency Ω between the probe and the control fields. As a result, thermo-optical oscillations are coherently induced in the cavity, tuning the optical resonator and thereby modulating the intracavity field at exactly the same frequency Ω . This leads to an interference that yields either a cancellation or an increase of the intracavity probe field depending on the relative phase between the two coherent fields, which results in a suppression or an amplification for the probe transmission. However, due to the slow thermal dissipation rate of the cavity, the coherent thermo-optical oscillations may occur with appreciable amplitude only if $\Omega \sim \gamma_{th}$. This condition determines the frequency bandwidth over which the phenomenon is observed, and suggests that the narrowness of the resulting spectral feature can, in principle, be strongly decreased by reducing the thermal dissipation rate of the cavity.

More formally, we can analytically capture the essence of this behaviour in terms of a simplified model in which the cavity is assumed to be uniformly heated by the thermal field, and heat is dissipated with a single decay rate from the cavity region.

Here we consider two coupled equations for the complex intracavity field amplitude, $a(t) = \bar{a} + \delta a(t)$, and the temperature variation, $\Delta T(t) = \bar{\Delta T} + \delta T(t)$, over the whole cavity volume:

$$\frac{da}{dt} = \left(i\omega_0 - \frac{\Gamma}{2} \right) a(t) + iG\Delta T(t)a(t) + \sqrt{\eta\Gamma} s_{in}(t) \quad (1a)$$

$$\frac{d(\Delta T)}{dt} = \beta|a(t)|^2 - \gamma_{th}\Delta T(t) \quad (1b)$$

¹Notice that for sufficiently intense control fields, the cavity eventually enters a thermo-optical bistable regime, settling to one of the two stable equilibrium points depending on the sign and value of Δ (13).

The first is the equation of motion for the driven cavity mode amplitude containing the input field, $s_{in}(t) = \bar{s}_{in} + \delta s_{in}(t)$, coupled to the cavity with efficiency η . The second equation describes the heat-flow from the cavity, which is characterized by a heat capacity C_p , and an effective thermal conductivity K , such that $\gamma_{th} = K/C_p$. Here, $\beta = \Gamma_{abs}/C_p$, where Γ_{abs} is the cavity linear absorption rate, and Γ is the full-width at half-maximum of the optical cavity resonance. The intracavity field, the temperature variation, and the input field are given by the sum of a strong mean-field due to the control laser and a weak modulation, due to the probe laser. With this ansatz, the coupled differential equations can be solved analytically in the steady state by linearizing with respect to the modulation amplitudes, $\delta s_{in}(t) = s_p e^{-i\Omega t}$, $\delta a(t) = A_p^- e^{-i\Omega t} + A_p^+ e^{+i\Omega t}$ and $\delta T(t) = T e^{-i\Omega t} + T^* e^{+i\Omega t}$, respectively. The solution displays an oscillation of the output power $I(t) = \eta\Gamma|a(t)|^2$ at frequency Ω , which can be interpreted as the optical beating between the intracavity probe and control field. We derived a compact and convenient expression for the oscillating component of $I(t)$:

$$\tilde{I} = \left(1 - \frac{\Gamma_{TOIT} - \gamma_{th}}{-i\Omega + \Gamma_{TOIT}}\right) \cdot \frac{2\bar{a}^* (\eta\Gamma)^{3/2}}{i(\bar{\Delta} - \Omega) + \Gamma/2} \cdot s_p \quad (2)$$

in which:

$$\Gamma_{TOIT} = \gamma_{th} \left(1 + \frac{|\bar{a}|^2}{|\bar{a}_b|^2} \tilde{\chi}(\bar{\Delta})\right) \quad (3)$$

and $|\bar{a}_b|^2 = -\frac{K\Gamma}{2G\Gamma_{abs}}$ represents the characteristic energy of the optical bistability threshold, while we defined $\tilde{\chi}(\bar{\Delta}) = \frac{4\bar{\Delta}/\Gamma}{4\bar{\Delta}^2/\Gamma^2 + 1}$ as a thermo-optical response function. The second multiplicative term on the right-hand side of Eq. (2) represents the response of the bare resonator to the probe field δs_{in} , while the term enclosed in brackets describes a narrow spectral hole, or anti-hole, with half-width half-maximum Γ_{TOIT} and visibility $|\mathcal{V}|$, such

that:

$$\mathcal{V} = 1 - \frac{\gamma_{th}}{\Gamma_{TOIT}} \quad (4)$$

for $\Gamma_{TOIT} > 0$, both dependent on the pump detuning and intensity, in which $\mathcal{V} > 0$ for the induced absorption regime, and $\mathcal{V} < 0$ otherwise. The resulting effect draws strict analogies with EIT and OMIT, respectively. However, the induced transparency is here due to a first-order system response, namely the thermal decay, that does not rely on any electronic or mechanical resonance, rather on the thermal field dissipated through the whole microcavity volume.

In resonators with negative thermo-optic coefficient ($\alpha < 0$) a spectral hole (induced absorption) is predicted at blue detuning regime ($\bar{\Delta} > 0$), with a linearly increasing linewidth as a function of the control beam power and visibility asymptotically approaching unity. Conversely, a spectral anti-hole (induced amplification) is expected at red-detuning regime ($\bar{\Delta} < 0$), whose spectral width decreases by increasing the control power, eventually approaching zero for $|\bar{a}|^2 = |\bar{a}_b|^2$, with diverging peak visibility. In both conditions, the value of $\tilde{\chi}(\bar{\Delta})$ and hence the visibility are maximized for $\bar{\Delta} = \pm\Gamma/2$. The calculated probe spectral response is shown in Fig. 1c for the red- and blue-detuning regimes, respectively.

The analytic relation between the real and imaginary parts of Eq. (2) links the existence of a sharp spectral dip (peak) to a steep phase response for $\Omega \ll \Gamma_{TOIT}$. This is associated to large group delay (advance), whose maximum value is given by $\tau_g = \mathcal{V}/\gamma_{th}$. The outgoing wave is delayed ($\tau_g > 0$) whenever a spectral dip is observed, while the maximum group delay is determined by the thermal response time (and hence by the thermal dissipative properties of the specific resonator structure). Conversely, high group advance ($\tau_g < 0$) can be achieved in the amplification regime, owing to the narrowing of the spectral feature. It should be remarked that the bandwidth of the process is reduced

under this driving condition, and thus the delay-bandwidth limit (and hence causality) is not violated. The maximum peak visibility and group advance achievable are in practice limited by the emergence of thermal bistability, which makes some combinations of pump power and detuning experimentally inaccessible due to the unstable nature of the thermo-optical equilibrium point (13).

3 Experiment

The model described in the previous section is not specific to a particular cavity design or material platform, indicating the general nature of the effect. The TOIT effect is most interesting in microresonators where the thermal response can vary over very different timescales, allowing a flexible trade-off between delay and bandwidth. The silicon photonics platform is very promising as there are a range of means to tailor the rate at which heat is dissipated, yielding different options for integration that provide a route to applications. Here we experimentally demonstrate TOIT using a two-dimensional photonic crystal (PhC) cavity (Fig. 1b), based on a dispersion-adapted line-defect design (14) and realized in a suspended silicon membrane. A simulation of the localized optical mode is shown superimposed to a micrograph of the sample, together with the associated temperature field profile generated by light absorption in the material.

The cavity was probed by coupling the control and probe fields in a resonant scattering (RS) reflection geometry (15). This allowed us to strongly suppress any spurious signals from the field reflected off the photonic crystal surface substrate and to easily isolate the field that interacted with the cavity.

The optical properties of the device (ω_0, Γ, η) were investigated by linear (low-power) spectroscopy, while its thermal properties (C_p, K) were estimated by finite-element method (FEM). The thermo-optic coefficient α and the absorption rate Γ_{abs} were estimated by

$\omega_0/2\pi$	193.61 THz
$\Gamma/2\pi$	5.09 GHz
η	0.038
C_p	1.6×10^{-11} J/K
K	3.9×10^{-5} W/K
$\gamma_{th}/2\pi$	0.38 MHz
α	-5.85×10^{-5} K $^{-1}$
Γ_{abs}/Γ	0.64

Table 1: Physical parameters estimated for the microcavity.

temperature-dependent spectroscopy and bistability trends, respectively. The extracted values are summarized in Table 1. We notice that typical values of $\gamma_{th} = K/C_p$ reported for nanoscale silicon photonic crystal cavities are as high as $\gamma_{th}/2\pi \sim 1$ MHz (16, 17), due to the extremely small value of C_p deriving from a diffraction-limited mode volume and the large value of K provided by the surface area of the photonic crystal.

In order to link the experimental results to our analytic model and quantitatively capture all the essential features of the TOIT phenomenon, the use of a single thermal decay rate assumed in the simplified model of two coupled Eqs. (1) is a too crude approximation. To fully understand the thermal response of the system, we have developed a numerical description of the heat diffusion problem within the PhC microcavity, which yields the distribution of ΔT as a function of both spatial coordinates and time (18). The spatially varying temperature is then linked to the optical length of the cavity, and we see that the silicon photonics platform is capable of accessing the induced transparency regime using coupled pumping powers of the order of few microwatts, as opposed to the hundreds milliwatts and bench-top systems previously used. However, including this full thermal description into the above rate equations would hinder the possibility to obtain an analytic solution to the problem. Therefore, in line with previous suggestions (13, 19), we developed a refined version of Eqs. 1, by introducing up to three interacting heat ca-

pacities, thus providing an approximation of the thermal response of the system but still allowing for an analytic solution. The use of three different heat capacities approximates correctly the description provided by our numerical simulation (18) and can be intuitively justified by considering that heat is generated in the very small modal volume of the microcavity through optical absorption, then it rapidly diffuses through the PhC lattice around the cavity, and it is eventually dissipated to the surroundings.

To observe the TOIT phenomenon, we excited the system with a strong control laser, while the weak probe was created by frequency shifting a fraction of the control beam through a cascade of two acousto-optic modulators. This way, we were able to scan the probe across the control within a $\Omega/2\pi$ range between -25 and 25 MHz. The optical beat note between the control and the probe was recorded at the input and output channels of the RS apparatus by two low-noise photodetectors and used to feed the reference and signal channels of a RF lock-in amplifier, in order to reconstruct the output power (Eq. 2) both in amplitude and phase. During each scan, the total RS signal was used to assess the detuning $\bar{\Delta}$ between the control field and the hot cavity mode (Fig. 2a, inset).

Each frequency scan was performed at fixed control power and detuning. For each value of control power, several spectra at different detuning conditions were acquired: an example of the overall result of such a measurement is summarized by the amplitude color scale plot in Fig. 2b, while the associated phase plot is shown in Fig. 3c. The maximum laser power used was limited to 7 mW in order to keep the contribution from nonlinear absorption processes (i.e., two-photon absorption and associated free-carrier absorption) negligible compared to linear absorption.

Figure 2a shows the recorded amplitude spectra for 4 mW control power (horizontal slices of Fig. 2b), and control frequency varying between 193.593 THz and 193.609 THz. In the presence of thermo-optic effect, the total RS power follows a characteristic sawtooth-

shaped response (inset in figure). A very narrow (\sim MHz) spectral feature, centered at $\Omega = 0$ was clearly observed, with a crossover from absorption to amplification regime associated to the crossing of the hot resonance, which is clearly evidenced in the color scale plot.

Similarly, Fig. 3a shows the associated phase spectra, which exhibit a sharp dispersive response in correspondence of the center of the spectral (anti-)hole. Notice that the phase derivative is positive in the induced absorption regime (upper panel) and negative in the induced gain regime (lower panel), and reaches its maximum absolute value for $\Omega = 0$.

Model fits to the experimental data are shown as solid black curves in Fig. 2a and 3a, respectively. The fitting algorithm was fed with the full lock-in trace, considering amplitude and phase response simultaneously for each experimental spectrum. The model used was based on a three heat capacities discretization, with associated decay rates $\gamma_{1,1}/2\pi = 1.77$ MHz, $\gamma_{2,2}/2\pi = 0.58$ MHz and $\gamma_{3,3}/2\pi = 0.11$ MHz. The theoretical value predicted by the non-refined model, $\gamma_{th}/2\pi = 0.38$ MHz (Table 1), can be interpreted as an effective parameter, which fits well within the range of the estimated decay rates. In order to further validate the adherence of the model to the cavity thermo-optical dynamics, we compared our results with temporally-resolved step-response measurements of the cold cavity as a function of the control detuning Δ .

Figure 2c shows the dip (peak) visibility, as defined by Eq. (4), as a function of $|\bar{a}|^2\tilde{\chi}(\bar{\Delta})$, calculated for all the acquired datasets. The experimental cavity energy $|\bar{a}|^2$ and detuning $\bar{\Delta}$ were estimated from best-fit of the bistable RS traces (Fig. 2a, inset). From these data, we derived the ratio $\Gamma_{TOIT}/\gamma_{th}$, shown in Fig. 2d. Both plots show a clear trend that is correctly fitted by a hyperbola and a linear regression, respectively, yielding a characteristic bistability energy $|\bar{a}_b|^2 = 0.2$ fJ, in agreement with the result obtained from the measurement of the resonance shift as a function of the incident power.

Finally, Fig. 3d relates the measured visibility to the maximum phase shift recorded within each scan. According to Eq. (2), this is expected to follow the relation:

$$\Delta\phi = 2 \arctan \frac{1}{2} \frac{\mathcal{V}}{\sqrt{1 - \mathcal{V}}} \quad (5)$$

Even in the framework of our refined model, this dependence correctly fits the data (solid line) up to a multiplicative factor ($\zeta \approx 0.58$).

To illustrate the potential of the TOIT phenomenon, we finally discuss the slow and fast light effects associated. As a consequence of the driven thermo-optical oscillations, a refractive index change is produced across the extremely narrow frequency range of the spectral feature, which implies that very large values (either positive or negative) of the group delay are expected for a probe frequency $\Omega \sim \gamma_{th}$. The measured group delay, defined as $\tau_g = \frac{d\phi}{d\Omega}$, is shown in Fig. 3b as a function of the beating frequency Ω . The experimental points are calculated from finite differentiation of the experimental data in Fig. 3a. Solid curves are best fits to our model, and clearly show a peak value for $\Omega \approx 0$. Negative values are associated to group advance, which is encountered in the gain regime.

Fig. 3e shows the maximum group delay (advance) as a function of the estimated visibility \mathcal{V} . The linear relation predicted by the previously introduced expression for τ_g is clearly satisfied, as shown by a linear fit of the experimental results. This yields an effective thermal decay rate $\gamma_{th}^{eff}/2\pi = 0.21$ MHz, in good agreement with the theoretical prediction, which corresponds to a maximum group delay of $\tau_g^{max} = 0.76$ μ s achievable in the blue-detuning regime.

4 Discussion and conclusions

First, we note that the maximum delay observed in our experiments, $\tau_g = 0.5$ μ s, has associated with it a loss of 5 dB and bandwidth of $2\pi \times 0.21$ MHz. This yields a delay-

bandwidth product of 0.66 and a loss per unit time of $10 \text{ dB } \mu\text{s}^{-1}$, orders of magnitude better than typical loss rates in integrated photonic devices (in the dB ns^{-1} range). We therefore now compare our system to other EIT analogues. Here we establish that for BSIT and OMIT the achievable linewidth and delay are given by the intrinsic linewidth/loss rate of an acoustic mode or mechanical resonance respectively. These properties are difficult to control and improve beyond values already presented in the literature. On the other hand, the heat transfer is comparatively simple to engineer and thus much larger delays are possible. E.g. in Ref. (14) a delay on the millisecond-range, with a linewidth of a few Hz, was demonstrated using a large and thermally isolated table-top setup, with a delay-bandwidth product comparable to our work. Furthermore, the engineering of thermal energy flow from PhC cavities is a well-studied problem, where the heat flow rate can be increased, through the inclusion of additional materials, for example, graphene (20) or reduced by structuring the surrounding material (18). In Ref. (18) we present a numerical model for the accurate description of the thermo-optic response of a cavity such as the one studied here under a constant pump scenario and show that structuring of the surrounding medium can engineer the heat flow out of the cavity. Applied to the TOIT effect we here show an example where support bridges are used to thermally isolate the PhC membrane from the remainder of the sample, reducing the thermal decay rate – and hence the transparency linewidth by more than one order of magnitude. Accordingly, the maximum theoretical delay increases by the same factor. This heat flow engineering is decoupled from the optical responses as the modifications takes place sufficiently far away from the electromagnetic field of the cavity that optical properties (such as the quality factor, mode volume, resonance wavelength etc.) are not affected. This contrasts other induced transparency phenomena, e.g. OMIT, where changing the mechanical resonance linewidth will typically also alter the optical properties of the cavity. In addition to changing

the thermal conduction properties of the device the heat capacity of the resonator can also be engineered, e.g. by using larger resonant devices such as micro-ring resonators. Lastly, we will address an issue inherent to all induced transparency phenomena. Induced transparency is a resonant process and as such, the theoretical delay-bandwidth product is limited to $\tau_g \Gamma_{ OMIT } = 1$. In conventional resonant systems, this can be overcome by either time-dependent control of the cavity (21) or the cascading or coupling of cavities and can in principle become arbitrarily high (22,23). The same can in principle be applied to induced transparency systems. However, the technological challenges associated with this are prohibitive for most implementations. In the case of OMIT, this would require the exact matching of both the mechanical and optical resonance frequency of multiple high Q-factor cavities. For TOIT on the other hand only the optical resonance wavelengths need to be matched (within the cavity linewidth) and the ability to use moderate Q-factor cavities - 38,000 vs 500 million (12) or 26 million (9) – greatly simplifies this task, which can be easily and accurately performed after the device fabrication (24). Therefore, as sketched in Fig. 3f, we can easily imagine multiple integrated cavities, cascaded along a waveguide that allow a larger delay for broader signals than achievable with a single resonant or induced transparency system.

We have reported on the experimental evidence and a detailed theoretical understanding of a new form of electromagnetically induced transparency occurring in a silicon integrated photonic platform at room temperature. The new phenomenology relies on the the slow thermo-optical response of a photonic crystal resonator, and manifests itself as a narrow spectral window of anomalous dispersion induced by control-probe interference within the cavity, which yields group delays or advances in the order of microseconds. The delay and bandwidth of this system can be tailored to specific application requirements by controlling the thermal properties of the cavity, independent of its optical properties,

or by cascading multiple cavities in a row, each exhibiting a TOIT window. The TOIT is fully compatible with chip integration using CMOS fabrication and operates at room temperature. The modest cavity Q-factors and low pump powers used makes the TOIT approach to induced transparency and amplification easy to implement and scalable, providing a route to the widespread use of large and controllable optical delays in integrated photonics.

References

1. M. Fleischhauer, A. Imamoglu, J. P. Marangos, *Rev. Mod. Phys.* **77**, 633 (2005).
2. K.-J. Boller, A. Imamoğlu, S. E. Harris, *Phys. Rev. Lett.* **66**, 2593 (1991).
3. L. V. Hau, S. E. Harris, Z. Dutton, C. H. Behroozi, *Nature* **397**, 594 (1999).
4. J. J. Longdell, E. Fraval, M. J. Sellars, N. B. Manson, *Phys. Rev. Lett.* **95**, 063601 (2005).
5. M. S. Bigelow, *Science* **301**, 200 (2003).
6. Q. Xu, *et al.*, *Phys. Rev. Lett.* **96**, 123901 (2006).
7. C. H. Dong, *et al.*, *Nat. Commun.* **6**, 6193 (2015).
8. G. S. Agarwal, S. Huang, *Phys. Rev. A - At. Mol. Opt. Phys.* **81**, 4 (2010).
9. S. Weis, *et al.*, *Science* **330**, 1520 (2010).
10. A. H. Safavi-Naeini, *et al.*, *Nature* **472**, 69 (2011).
11. H. Zhang, *et al.*, *Appl. Phys. Lett.* **100**, 131102 (2012).
12. J. Ma, *et al.*, *Science Advances* **6** (2020).

13. T. Carmon, L. Yang, K. J. Vahala, *Opt. Express* **12**, 4742 (2004).
14. K. Welna, S. L. Portalupi, M. Galli, L. O'Faolain, T. F. Krauss, *IEEE J. Quantum Electron.* **48**, 1177 (2012).
15. M. Galli, *et al.*, *Appl. Phys. Lett.* **94**, 1 (2009).
16. T. Tanabe, M. Notomi, S. Mitsugi, A. Shinya, E. Kuramochi, *Opt. Lett.* **30**, 2575 (2005).
17. L.-D. Haret, T. Tanabe, E. Kuramochi, M. Notomi, *Opt. Express* **17**, 21108 (2009).
18. S. Iadanza, *et al.*, *Phys. Rev. B* **102**, 245404 (2020).
19. V. Ilchenko, M. Gorodetsky, *Laser Phys.* **2**, 1004 (1992).
20. M.-H. Shih, *et al.*, *ACS Nano* **7**, 10818 (2013).
21. Q. Xu, P. Dong, M. Lipson, *Nat. Phys.* **3**, 406 (2007).
22. S. A. Schulz, *et al.*, *J. Opt.* **12**, 104004 (2010).
23. I. Cardea, *et al.*, *Sci. Rep.* **10**, 15752 (2020).
24. M. Clementi, A. Barone, T. Fromherz, D. Gerace, M. Galli, *Nanophotonics* **9**, 205 (2019).

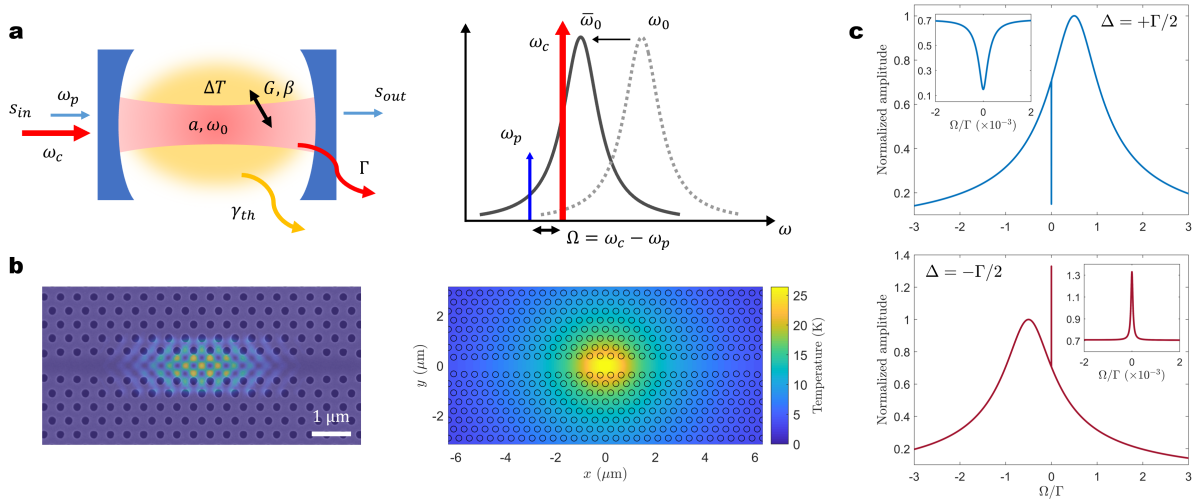


Figure 1: control-probe of a thermo-optical cavity. **a.** (left) Schematic of the thermo-optical cavity, showing the fields and the main physical quantities involved. (right) Thermo-optically shifted resonance (blue-detuning regime) as a static effect of the control field. **b.** (left) Scanning electron micrograph and simulated optical field of the photonic crystal cavity used for the experiment. The optical mode localizes at the widest point of the line-defect. (right) Simulated thermal distribution for a stationary absorbed power $P_{abs} = 1$ mW in correspondence of the cavity mode. **c.** Calculated pump-probe response from the steady state solution of the equations of motion, showing the output power \tilde{I} as a function of the pump-probe detuning frequency Ω , in the amplification (red pump-cavity detuning, *bottom*) and absorption (blue pump-cavity detuning, *top*) regimes, respectively. The broad resonance represents the bare cavity mode, while the narrow spectral feature (inset) at zero pump-probe detuning is due to the thermo-optical nonlinearity.

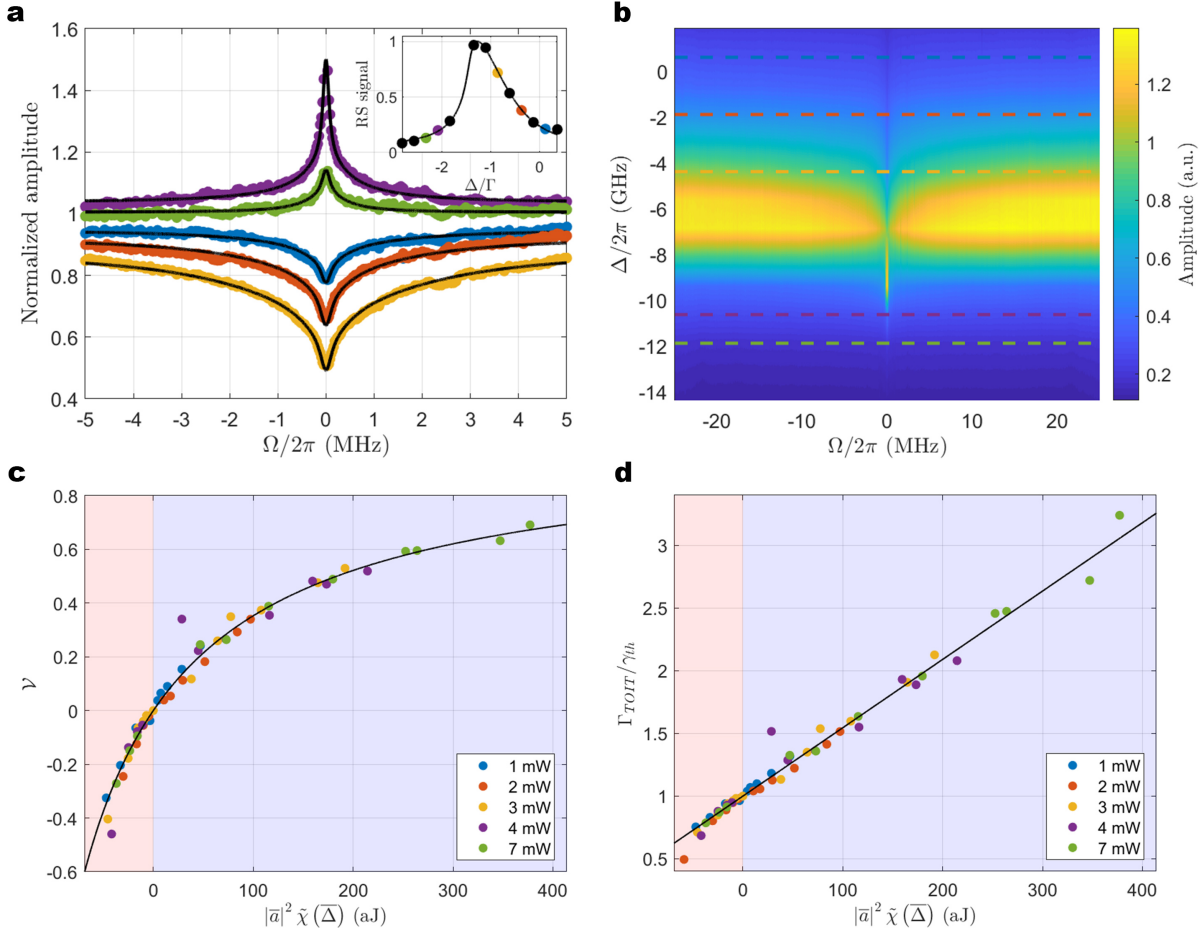


Figure 2: Highly resolved amplitude response. **a.** Normalized resonant scattering spectra (dots) and model fit (black curve) for the output power \tilde{I} as a function of the control-probe detuning frequency Ω for a nominal control power $P = 4$ mW. The traces are normalized on the average value measured at $\Omega/2\pi = \pm 25$ MHz. (inset) Time-averaged RS power collected during each scan (dots) and best fit with a bistable nonlinear model (black curve). Colored points correspond to measured spectral traces and provide detuning conditions, $\bar{\Delta}$, and coupled power, $|\bar{a}|^2$. **b.** Intensity plot of the output power \tilde{I} as a function of the control-probe detuning frequency and control-cavity detuning $\Delta = \omega_c - \omega_0$. Horizontal slices correspond to experimental traces in panel a. **c.** Dip (blue region, positive values) and peak (red region, negative values) visibility as a function of the product $|\bar{a}|^2 \tilde{\chi}(\bar{\Delta})$. The visibility is calculated from a best fit of the experimental spectra for the whole experimental dataset. The legend reports the nominal laser power for each measurement. **d.** Linewidth broadening (narrowing) as a function of $|\bar{a}|^2 \tilde{\chi}(\bar{\Delta})$. The values on the vertical axis are calculated upon the data in panel c as $\Gamma_{TOIT}/\gamma_{th} = 1/(1 - \mathcal{V})$.

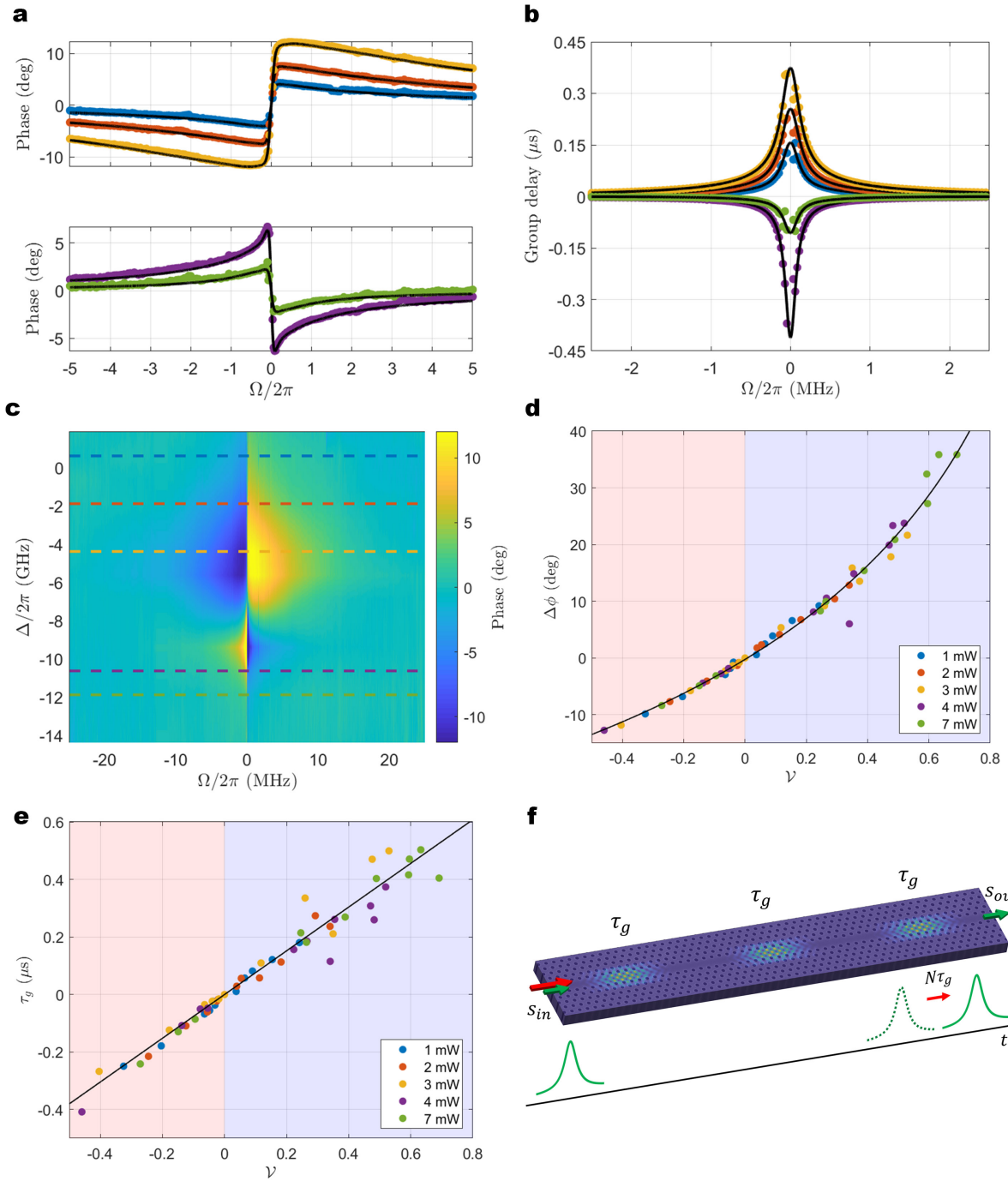


Figure 3: Phase response. **a.** Probe phase spectra as a function of the control-probe detuning frequency, Ω . The experimental data (dots) and model fit (black curve) represent the phase trace associated to the amplitude response shown in Fig. 2a. Upper and lower panels correspond to blue- and red-detuning condition respectively. **b.** Group delay traces obtained by numerical differentiation of data shown in panel a. **c.** Intensity plot of the measured phase as a function of the control-probe detuning frequency Ω and control-cavity detuning $\Delta = \omega_c - \omega_0$, associated to the measurement shown in Fig. 2b. Horizontal slices correspond to experimental traces in panel a. **d.** Maximum phase shift and **e.** peak group delay (advance) as a function of ν . The blue (red) region correspond to the absorption (amplification) regime. Black curves are model fit to data. **f.** Conceptual scheme for cascaded TOIT. The group delay τ_g induced by the N microcavities sums to the overall value $N\tau_g$, overcoming the time-bandwidth limit which holds for the single microresonator.